Spectral coherence properties of continuum generation in bulk crystals

Benjamin Maingot, Gilles Chériaux, Nicolas Forget, Aurélie Jullien

Research Article | Vol. 30, No. 12 / 6 Jun 2022 / Optics Express 20311
Optics EXPRESS

Spectral coherence properties of continuum generation in bulk crystals

BENJAMIN MAINGOT,[1,2,*] GILLES CHÉRIAUX,[1] NICOLAS FORGET,[2] AND AURÉLIE JULLIEN[1]

[1] *Institut de Physique de Nice (INPHYNI), Université Côte d'Azur, CNRS, UMR 7010, 1361 route des Lucioles, 06560 Valbonne, France*
[2] *Fastlite, 165 route des Cistes, 06600 Antibes, France*
[*] *benjamin.maingot@fastlite.com*

Abstract: The stability of the phase difference between two white-light continua, generated from the same 180-fs pulses at ≃1035 nm, is assessed by a modified Bellini-Hänsch interferometer. Mutual spectral phase stability is studied and quantified as a function of several parameters: pulse energy, position of the nonlinear crystal with respect to the beam waist and interaction length. Our results show that intrapulse decoherence may significantly contribute to the measured CEP noise floor. In addition, spectrally-resolved intensity-to-phase coupling coefficients are measured and stability regions are identified.

1. Introduction

Third-generation femtosecond sources [1] can deliver wavelength-tunable, high average power, few-cycle pulses with not only a reproducible intensity but also a reproducible electric-field. The latter has proven to be an essential feature for field-driven phenomena such as in attosecond physics [2–4]. A prerequisite to field control is to stabilize the phase between the optical carrier and the amplitude envelope (CEP, for carrier-envelope phase). Nonlinear optics provide an elegant and robust way to generate CEP-stable seeds, especially via the difference frequency generation (DFG) between two waves sharing the same phase fluctuations [5,6]. So far, even if record long-term CEP noise as low as 65 mrad rms [7] has been demonstrated, the origin and level of the CEP noise floor remains an open question.

Third-generation sources rely on white-light continuum generation (WLG) to extend the spectrum of picosecond or sub-picosecond optical pump pulses, so as to allow DFG between the pump pulses and a visible- or infrared-wing of a single filament. By focusing μJ-level 1030 nm pulses in a nonlinear transparent crystal such as YAG, a broad and stable spectrum extending from the visible to >1.5 μm can be sustained [8,9]. Among the essential properties of WLG is the pulse-to-pulse phase relationship between the spectral components of the continuum, which may be referred to as the intrapulse coherence [10]. Intrapulse coherence plays an essential role in pulse compression and decoherence can be a source of CEP noise. As pointed out by numerical simulations, the plasma contribution in filaments could be a major source of loss of intrapulse coherence [10], in contrast with supercontinuum generation in fibers [11,12]. As it is difficult to disentangle fundamental from technical noise in CEP measurements, because of the complexity and nonlinearity of the measurement process, an alternative approach is to assess the phase stability of the new frequency components generated by filamentation and to compare this lower bound with the lowest recorded CEP noise.

In this paper, we experimentally characterize the intrapulse coherence of a continuum generated in a thick YAG crystal by an amplified Ytterbium laser. The characterization method relies on a variant of the Bellini-Hänsch interferometer [13]: two identical WLGs are inserted in a balanced Mach-Zhender interferometer and the shot-to-shot phase fluctuations are analysed by spectral interferometry. Compared to former results, the proposed analysis is quantitative and extends

#459123 https://doi.org/10.1364/OE.459123
Journal © 2022 Received 30 Mar 2022; revised 12 May 2022; accepted 12 May 2022; published 23 May 2022

Optics EXPRESS

from the visible to the short infrared spectral range. Furthermore, as a complement to [10], the relative phase noise is frequency-resolved, continuously over the full spectral bandwidth, which makes application of our results not limited to CEP stabilization and measurement. The effects of seed energy, crystal position, and crystal length are assessed. From this multi-parameter study we define stability ranges for WLG, assess intensity-to-phase coupling coefficients [14], and identify an operating range in which these coefficients vanish.

2. Experimental methods

The generation parameters for WLG follows the general guidelines indicated by for sub-ps WLG [15]. We use Yttrium Aluminum Garnet (YAG) crystals and the seed laser is focused with a numerical aperture of 0.015 to optimize the generation of the infrared part of the spectrum. Two configurations are distinguished in this work, depending on the position of the crystal relatively to the laser focus. When the front face of the crystal is placed before the waist, the broadening is limited in the infrared and the visible wing of the continuum is broad and stable. When placed after the waist, the infrared wing is extended and the visible wing tends to become unstable. In addition, two crystal lengths are studied: 6 mm and 10 mm. Increasing the crystal length tends to increase the intensity and the width of the infrared spectrum.

The pump laser is a regenerative CPA system (Pharos, Light Conversion) delivering pulses at ≃1035 nm with a pulse duration of ≃180 fs FWHM. The beam diameter ($1/e^2$) is 4.5 mm with excellent beam quality (M^2=1.1). For these experiments, the repetition rate is set at 1

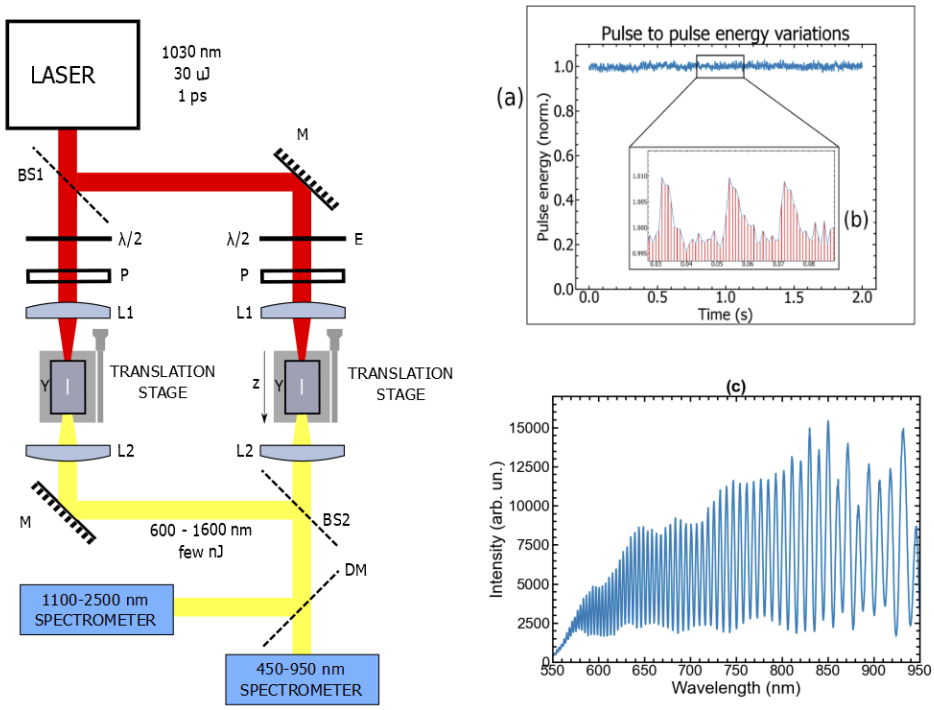

Fig. 1. Diagram of the interferometer. M: mirrors, BS1: 1030 nm 50/50 beam splitter, BS2: low GDD 600-1500 nm 50/50 beam splitter, $\lambda/2$: half wave plate, P: polarizer, L1: focusing lens f = 150 mm, L2: achromat focusing lens f = 50 mm, Y: YAG crystal, DM: dichroic mirror. (a) Pulse-to-pulse energy stability of the driving laser. (b) Zoom over 100 ms (each red bar is a laser shot). (c) Typical fringed spectrum from the short wavelength range.

Optics EXPRESS

Table 1. Different experimental configurations and parameter-scans performed in this study. z-scan (resp. E-scan) refers to a controlled change of the YAG position (reps. seed energy) in the test arm.

Exp. config.	YAG length	Position	Scan	Figures
I	6 mm		z-scan	4
II	6 mm	Before focus	E-scan	5,6
III	6 mm	After focus	E-scan	5,6
IV	10 mm	After focus	E-scan	
V	10 mm		z-scan	

kHz and ≃9 uJ are sampled from the available ≃1 mJ of pulse energy. The interferometer is of Mach-Zehnder type. Each arm includes a half-waveplate and a polarizer to adjust the pulse energy on each YAG crystal independently. A pair of f=150 mm lenses focus the beam in identical 6-mm-long YAG crystals (NA: 0.015) and f=50 mm achromatic lenses collimate the spectrally-broadened beams. One arm of the interferometer serves as a test arm whereas the other one is the reference arm (Fig. 1). The adjustable parameters in the test arm are reported in Table 1 of Fig. 1. Although not shown in Fig. 1, a reflective delay line controls the relative group delay of the two arms. Once recombined, the beams are focused into two array-based spectrometers: a 450-1100 nm Silicon spectrometer (resolution of 0.26 nm, integration time of 1.1 ms) and a 1000-2500 nm InGaAs spectrometer (resolution of 3.27 nm, integration time of 1 ms). These spectral ranges will be referred to as the short wavelength range and the long wavelength range.

For a relative group delay of a few hundreds of fs, the measured spectra show interference fringes over the full spectral range, as illustrated in Fig. 1(c). To study the relative phase stability, 1000 consecutive single-shot spectra are acquired and analyzed. From each single-shot interference spectrum, the spectral phase is extracted by a discrete Hilbert transform [16,17]. The standard deviation of the phase (σ) at each wavelength is then used as metric to assess the intrapulse coherence (Fig. 2). Prior to the computation of the standard deviation, a 5-Hz high-pass filter is applied to remove slow phase drifts. The rationale for this choice is that (i) most,

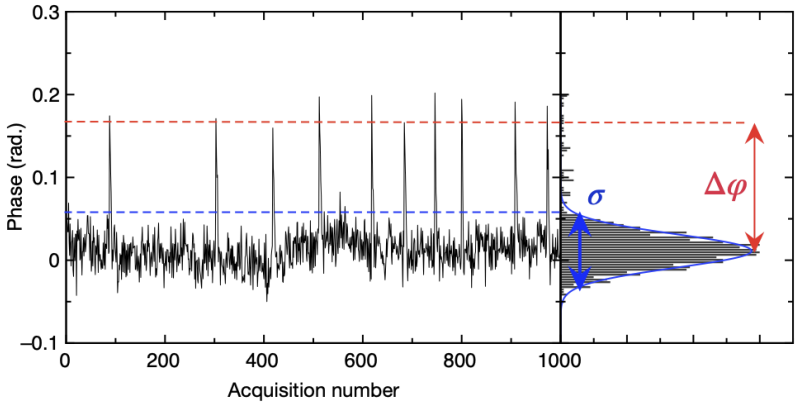

Fig. 2. Illustration of the significant quantities extracted from the acquisitions: the phase is calculated by Fourier transform for an arbitrarily chosen wavelength as a function of acquisition time for each acquired spectrum. The blue dashed line indicates the threshold applied to filter out the effect of laser overshoots (see text). σ is the standard deviation of the measured phase noise, and $\Delta\varphi$ is the phase jump induced by laser overshoots. The process is repeated for each wavelength.

Optics EXPRESS

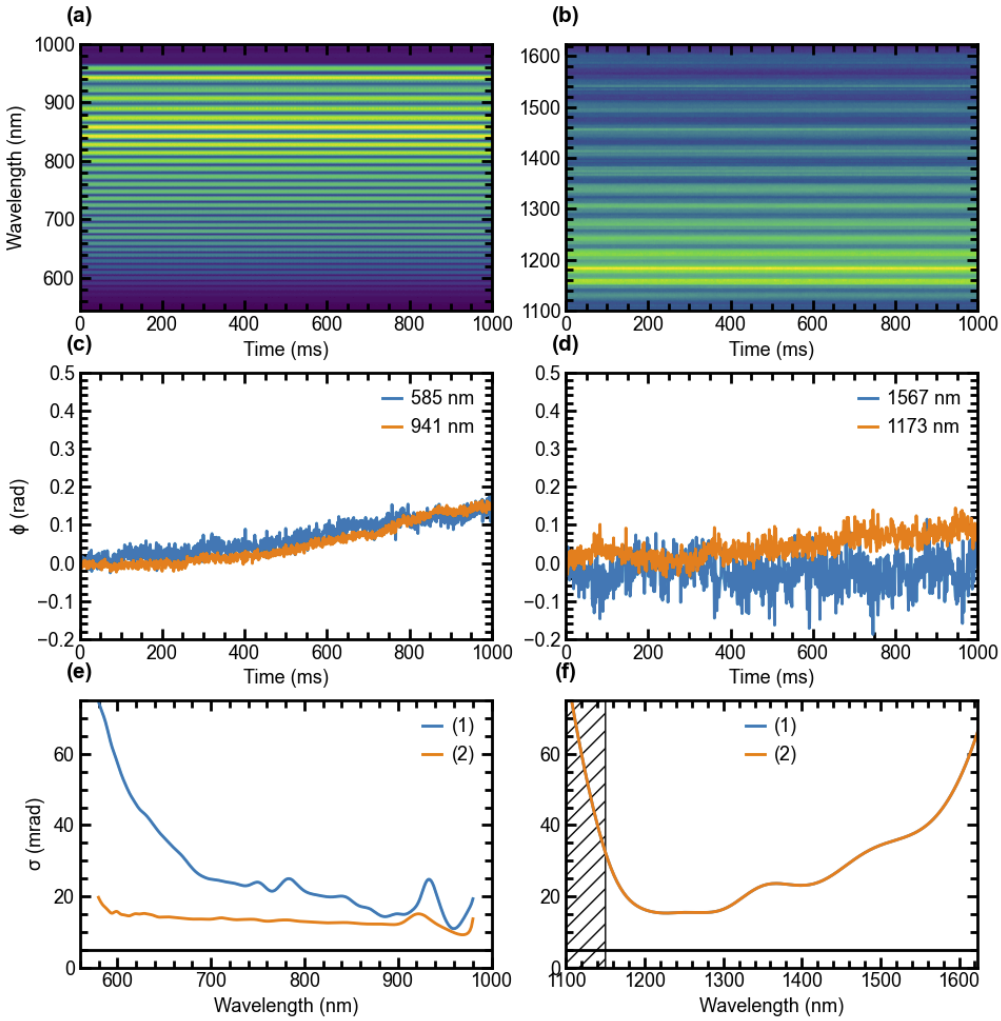

Fig. 3. (a,b) Typical spectrograms over 1000 single shot measurements, in the short (a) and long (b) wavelength range. (c,d) Retrieved phase from each acquisition, at two arbitrarily selected wavelengths in the short (c) and long (d) wavelength range. (e,f) Retrieved phase standard deviation as a function of wavelength with a 5 Hz high pass filter alone (1) and with an additional filtering on the fast energy peaks of the pump laser (2). The absorption window of silicon is also highlighted to discard the measurements in this range because of the low signal to noise ratio.

Optics EXPRESS

if not all, CEP-stable sources include a slow feedback loop [18], (ii) we focus on shot-to-shot phase fluctuations. Wavelengths for which the spectrometer noise equals or exceeds the detected level of light were discarded from this analysis.

The shot-to-shot energy stability of the Pharos system is shown in Figure 1(a). Despite an overall stability below 0.5% rms, 1% peak-to-peak fluctuations followed by a fast relaxation (i.e. over few laser shots) are observed (Figure 1(b)). These events appear randomly and this behaviour is not explained at this time. Here, we decided to study the contribution of these fluctuations separately from the stability analysis. Thus, the overall phase data set is divided into two distinct subsets. First, the stochastic phase noise is analyzed by filtering out the jumps due to energy overshoots, thanks to a threshold applied to the phase fluctuations. These data correspond to less than 10% of the total data volume, so filtering them does not affect the analysis (Fig. 2(b)). In a second step, the impact of a 1% peak-to-peak energy change is analyzed by measuring the spectrally-resolved amplitude-to-phase transfer coefficient [14].

To subtract the phase artifacts from the optics and assess the precision of the measurement, we proceed in two steps: (i) without YAG crystals and (ii) with YAG crystals and balanced WLGs. Without crystals the typical measured standard deviation is <5 mrad at 1030 nm, which provides a ground floor for the phase noise measurement. For (ii), the front face of the 6-mm YAG crystal is placed slightly before the waist with the energy set slightly below the double filamentation threshold. This configuration, which corresponds to the stable range of [14] is chosen as the operating point of the reference arm in the following. Figures 3(a) and 3(c) show the recorded spectrograms. Figures 3(b) and 3(d) show the respective phase stability with and without removing the 1% energy overshoots. Compared to the ground floor, the phase noise shows an expected increase due to the addition of nonlinearity, from <5 mrad to <20 mrad. The phase stability tends to decrease as the wavelength offset from the pump wavelength increases. The filtering on the laser overshoots has a stronger effect in the visible and almost no influence in the infrared, as will be detailed in the last section. Nevertheless, the stability remains excellent and this value of 20 mrad will be our reference for the later experiments.

3. Results

The first investigated parameter is the position of the YAG crystal along the propagation axis (I). Figure 4 shows the phase stability as a function of the crystal position for three selected wavelengths in the short wavelength range (Fig. 4(a)) and in the long wavelength range (Fig. 4(b)). The long wavelength side shows a wide stability range of 4 mm (from $z = 0.2$ to $z = 4.2$) with a phase noise below 20 mrad rms. Although the crystal position modifies the spectral shape, almost no influence on the phase noise is measured, except when the crystal is moved far from the waist. Conversely, the stability range for the short wavelength range is much narrower (1 mm around $z = 2$ mm). This range coincides with the generation of an intense, broad and stable spectrum in the visible. Out of this range, the phase noise tend to increase (at 700 nm especially), even if a second noise plateau can be identified at $z = 4$ mm.

To study the influence of pulse energy, both crystals are set to $z = 2$ mm (II) and then to $z = 4$ mm (III). For $z = 2$ mm (II), the energy is varied from 0.35 to 1.57 μJ (step of 20 nJ steps), that is, from the onset of filamentation to above the threshold of double filamentation (1.13 μJ). Double filamentation is easily identified via the deep modulation of the spectrum caused by the interference between the two filaments. Both short and large wavelength ranges display the same qualitative behavior: the phase noise first decreases and then increases with pulse energy (Fig. 5(a,b)). At low energy, there is not enough to establish a stable filament and intensity fluctuations have a higher impact on the phase. At some point, the filament is well established and adding more energy does not decrease the impact of the fluctuations anymore until there is enough energy to generate and additional filament after the first one. As identified in [14], the phase noise is low, 20 mrad rms for the visible range and 30 mrad rms for the IR range, when the

Optics EXPRESS

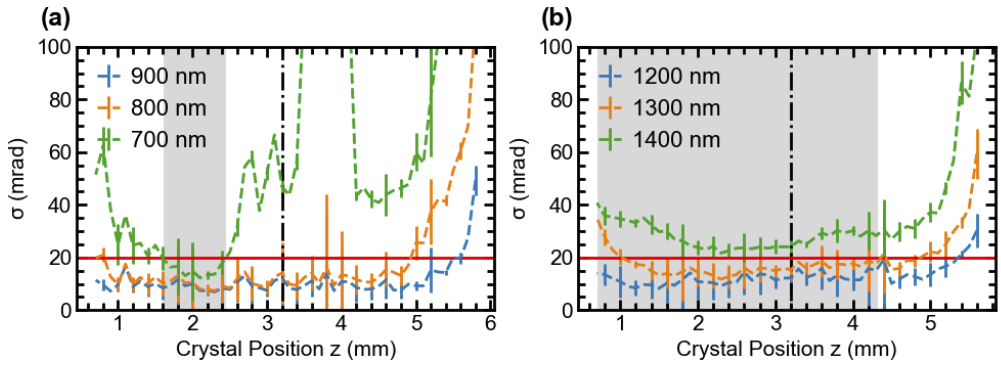

Fig. 4. (I) Phase standard deviation as a function of crystal position in the short (a) and long (b) wavelength range. The focus (z=3.2 mm) is indicated with a dashed line. Lower z-values values gets the YAG closer to the focusing lens while higher z-values are further away from the lens. The red line indicates the balanced stability of the interferometer. The grey areas refer to the stability operating zone.

single filament is stable. The stability range extends from 0.66 to 1.15 μJ in the short wavelength range and from 0.83 to 1.11 μJ in the long wavelength range. In both cases, the stability range extends up to the threshold of double filamentation.

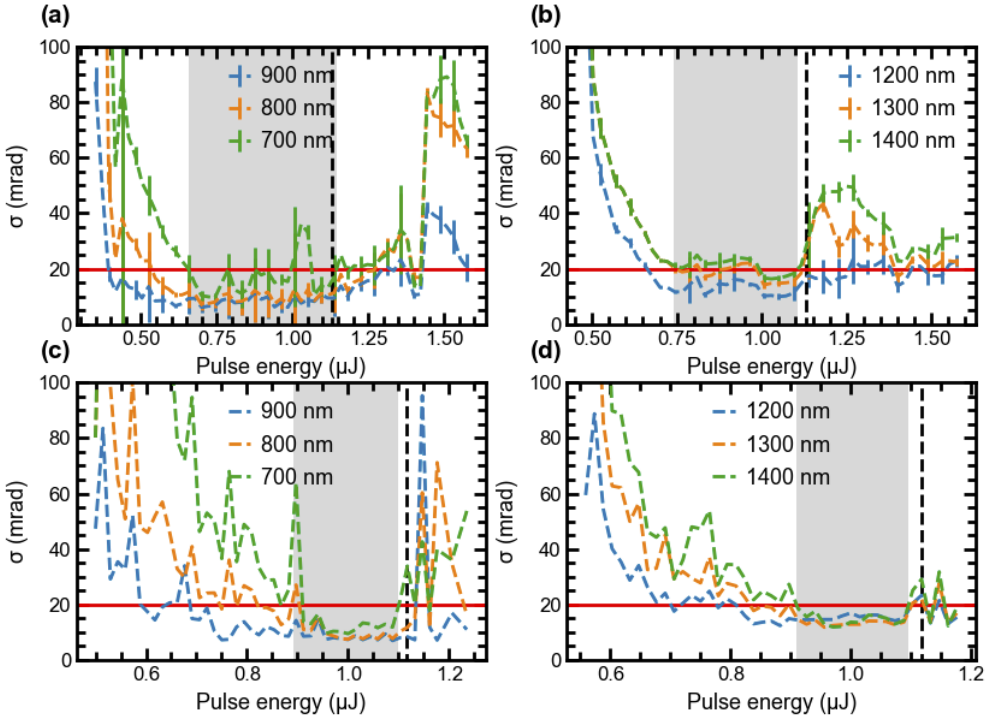

Fig. 5. Phase standard deviation as a function of seed pulse energy in the short (a, c) and long (b, d) wavelength ranges for $z = 2$ mm (II) and $z = 4$ mm (III) respectively. The energy axis starts at the onset of filamentation. The dotted black line refers to the onset of double-filamentation. The grey areas refer to the stability operating zone.

Optics EXPRESS

For $z = 4$ mm (III), which is the position for which the infrared wing is favoured, the energy was varied from 0.5 to 1.23 µJ (15 nJ steps). The results are very similar: noise decreases with increasing energy and reaches a stability plateau until double filamentation breaks in (Fig. 5(c,d)). However, as expected from Fig. 4(a), by comparison with configuration (II), the range where the noise is below 20 mrad is narrower in the short wavelength range (0.89 - 1.1 µJ) and slightly larger in the long wavelength range (0.79 - 1.1 µJ).

The last parameter studied in this paper is the crystal length. Here we compare a 6 mm crystal with a 10 mm crystal, all other parameters being equal. With a longer crystal, the infrared spectrum is broader and the infrared cut-off wavelength (measured at 20% of the maximum spectral density) increases from 1580 nm to 1720 nm. The behaviours are qualitatively similar. Table 2 gathers some significant phase stability values measured in this study. Stability range and minimum phase jitter are reported. The long wavelengths range shows better stability (i.e. larger stability ranges, lower minimal jitter) in all configurations but configuration (II). On the contrary, placing the YAG crystal before the waist (II) is the best for the short wavelengths range, as the stability range is almost twice as large in (II) than in (III). Increasing the crystal length (IV and V) shows no benefit on the stability.

Table 2. Significant phase stability values for the different experimental configurations : phase stability ranges for the two spectral bands (two first rows); minimum phase noise for two wavelengths (two last rows).

	I	II	III	IV	V
Stab. range (short λ)	1.6 - 2.5 mm	0.66 - 1.15 µJ	0.89 - 1.1 µJ	above 20 mrad	above 20 mrad
Stab. range (long λ)	0.7 - 4.32 mm	0.83 - 1.11 µJ	0.79 - 1.1 µJ	0.83 - 1.3 µJ	0.5 - 4.8 mm
min jitter @750 nm	12 mrad	9 mrad	9.5 mrad	28 mrad	21 mrad
min jitter @1300 nm	12 mrad	14 mrad	12 mrad	5 mrad	7 mrad

4. Intensity-to-phase transfer coefficients

Finally, the impact of the 1% energy overshoots (Fig. 1(b)), that were first filtered out, are analyzed. The intensity-to-phase coupling is actually visible in the spectrogram, as wavelength-dependent phase jumps ($\Delta\varphi$, Fig. 2) correlated to the seed energy fluctuations, as also shown in Fig. 6(a). Quantifying the intensity-to-phase coupling as a function of wavelength and of WLG regime is of interest for two reasons. First, it plays an important role in CEP-stable sources implementing pump amplitude modulation for CEP control in DFG-based systems [19]. Second, a stationary point can be identified.

We therefore extract the phase jumps values, related to the 1% energy laser fluctuations for all experimental configurations, and compute for these laser pulses the spectrally-resolved energy-to-phase transfer coefficient ($\kappa(\lambda)$). The results for experimental configurations II and III are shown in Figures 6(b) and 6(c), featuring $\kappa(\lambda)$ as a function of seed energy in the test arm. In both cases the infrared part of the continuum seems not to be affected by the intensity fluctuations, i.e. the transfer coefficient is close to 0. In the visible part of the spectrum, $\kappa(\lambda)$ is (i) larger when the energy is low or close to the onset of double filamentation, and (ii) larger for shorter wavelengths. The maximum value of κ is much larger for experimental configuration (III) than (II): 2 rad./% versus 0.6 rad./% at 650 nm, implying that WLG favorable to the short-wavelength generation is intrinsically more compatible with CEP-stable systems. Finally, in both configurations, a stationary point is identified when $\kappa(\lambda)$ vanishes across the whole spectrum at 0.785±0.085 µJ for configuration (II) and at 0.955±0.015 µJ for configuration (III). For the latter configuration, the stationary point lies just below the double-filamentation threshold. Somewhat counter-intuitively, the stationary point is narrower in (II) than in (III), despite a lower coupling coefficient, and a larger stability range for the stochastic noise.

Optics EXPRESS

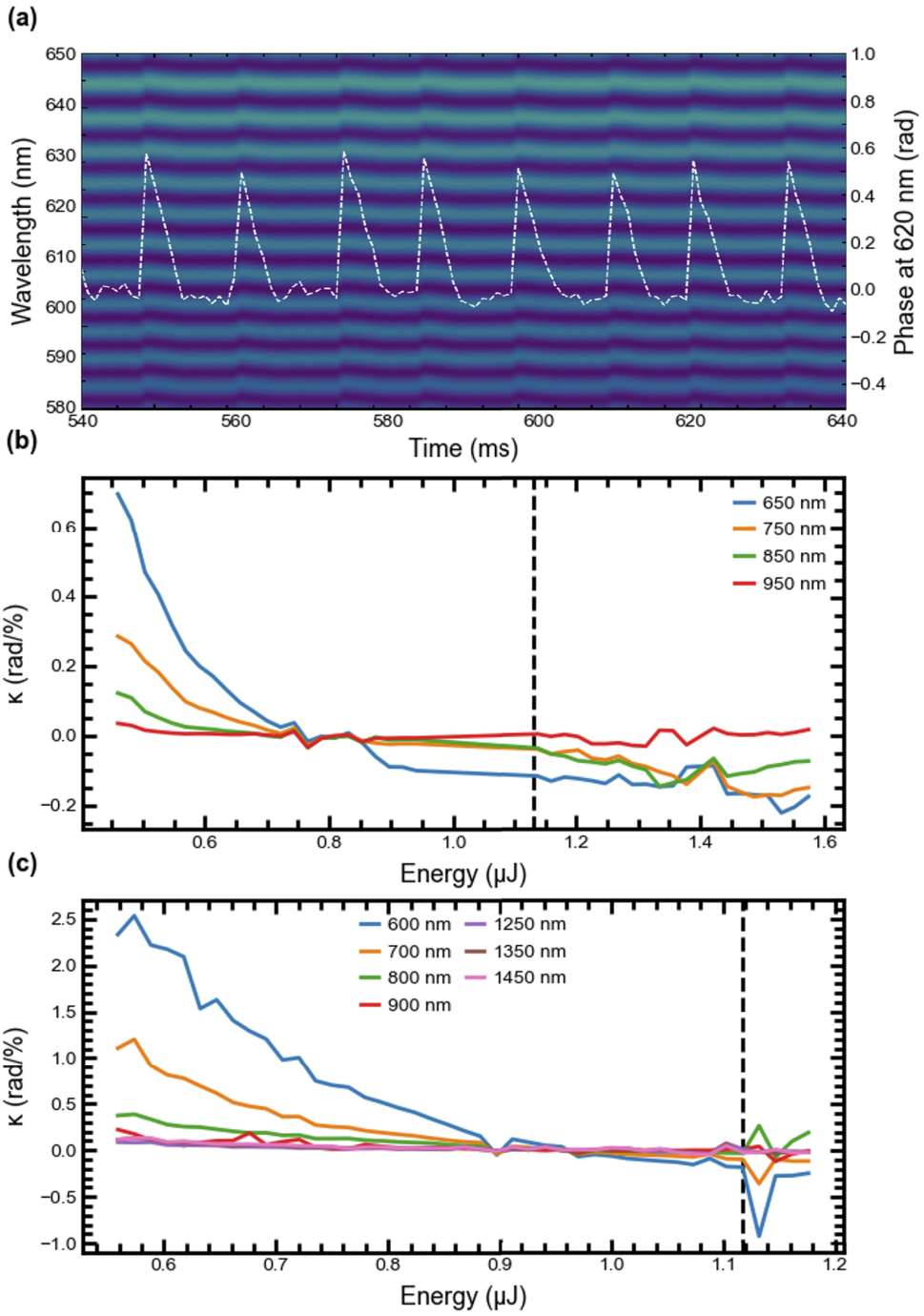

Fig. 6. (a) Spectrogram zoomed over 300ms and over 580 nm-650 nm spectral bandwidth so as to emphasize the phase fluctuations due to amplitude-to-phase coupling. The white dashed line is the retrieved phase at 620 nm. Amplitude-to-phase coupling coefficient for experimental configurations II (b) and III (c). The dashed black line refers to the onset of double-filamentation.

Optics EXPRESS

5. Conclusion

To conclude, by means of a modified Bellini-Hänsch interferometer, we characterized the stochastic fluctuations of the spectral phase of a continuum generated via the filamentation of ≃180 fs pulses at ≃1035 nm in YAG crystals. Compared to the original publication by Bellini and Hänsch [13], the analysis is quantitative, spectrally-resolved, and extended to the short-wave infrared. Lenient generation conditions have also been identified and it is found that even if the crystal position modifies the spectral shape, the spectral phase of the continuum remains stable across the full bandwidth for large range of positions. We have also quantified the chromatic dependency of the intensity-to-phase coupling coefficient. For all the studied configurations, we could identify an experimental configuration for which this coupling coefficient vanishes. In the context of CEP-stable sources, our results indicate that intrapulse coherence may contribute to the measured CEP noise, both at the DFG level and in the f-to-2f interferometer, to a level >10-20 mrad (each). Our results thus confirm that intrapulse decoherence may significantly contribute to the measured CEP noise floor and may even represent the major contribution in third-generation sources displaying a non-averaged CEP noise below ≃60 mrad. Beyond CEP stability, our results may also be of interest for pulse synthesis as well as for broadened frequency combs. These results could, however, depend on the characteristics of the driving laser, and, in particular, on wavelength, beam quality, temporal contrast and spectro-temporal stability.

Funding. European Regional Development Fund (OPTIMAL); Agence Nationale de la Recherche (ANR-19-CE30-0006-01); HORIZON EUROPE Framework Programme (GA860553).

Acknowledgments. The authors thank Günter Steinmeyer for fruitful discussion. The project leading to this application has received funding from the European Union's Horizon 2020 research and innovation programme under the Marie Sklodowska-Curie grant agreement No 860553.

Disclosures. The authors declare no conflicts of interest.

Data availability. Data underlying the results presented in this paper are not publicly available at this time but may be obtained from the authors upon reasonable request.

References

1. H. Fattahi, H. G. Barros, M. Gorjan, T. Nubbemeyer, B. Alsaif, C. Y. Teisset, M. Schultze, S. Prinz, M. Haefner, M. Ueffing, A. Alismail, L. Vámos, A. Schwarz, O. Pronin, J. Brons, X. T. Geng, G. Arisholm, M. Ciappina, V. S. Yakovlev, D.-E. Kim, A. M. Azzeer, N. Karpowicz, D. Sutter, Z. Major, T. Metzger, and F. Krausz, "Third-generation femtosecond technology," Optica **1**(1), 45–63 (2014).
2. P. á. Corkum and F. Krausz, "Attosecond science," Nat. Phys. **3**(6), 381–387 (2007).
3. S. R. Leone, C. W. McCurdy, J. Burgdörfer, L. S. Cederbaum, Z. Chang, N. Dudovich, J. Feist, C. H. Greene, M. Ivanov, R. Kienberger, U. Keller, M. F. Kling, Z.-H. Loh, T. Pfeifer, A. N. Pfeiffer, R. Santra, K. Schafer, A. Stolow, U. Thumm, and M. J. J. Vrakking, "What will it take to observe processes in'real time'?" Nat. Photonics **8**(3), 162–166 (2014).
4. J. Li, J. Lu, A. Chew, S. Han, J. Li, Y. Wu, H. Wang, S. Ghimire, and Z. Chang, "Attosecond science based on high harmonic generation from gases and solids," Nat. Commun. **11**(1), 1–13 (2020).
5. A. Baltuška, T. Fuji, and T. Kobayashi, "Controlling the carrier-envelope phase of ultrashort light pulses with optical parametric amplifiers," Phys. Rev. Lett. **88**(13), 133901 (2002).
6. G. Cerullo, A. Baltuška, O. D. Muecke, and C. Vozzi, "Few-optical-cycle light pulses with passive carrier-envelope phase stabilization," Laser Photonics Rev. **5**, 323–351 (2011).
7. N. Thiré, R. Maksimenka, B. Kiss, C. Ferchaud, G. Gitzinger, T. Pinoteau, H. Jousselin, S. Jarosch, P. Bizouard, V. Di Pietro, E. Cormier, K. Osvay, and N. Forget, "Highly stable, 15 w, few-cycle, 65 mrad cep-noise mid-ir opcpa for statistical physics," Opt. Express **26**(21), 26907–26915 (2018).
8. M. Bradler, P. Baum, and E. Riedle, "Femtosecond continuum generation in bulk laser host materials with sub-μj pump pulses," Appl. Phys. B **97**(3), 561–574 (2009).
9. A. van de Walle, M. Hanna, F. Guichard, Y. Zaouter, A. Thai, N. Forget, and P. Georges, "Spectral and spatial full-bandwidth correlation analysis of bulk-generated supercontinuum in the mid-infrared," Opt. Lett. **40**(4), 673–676 (2015).
10. N. Raabe, T. Feng, T. Witting, A. Demircan, C. Brée, and G. Steinmeyer, "Role of intrapulse coherence in carrier-envelope phase stabilization," Phys. Rev. Lett. **119**(12), 123901 (2017).
11. X. Gu, M. Kimmel, A. P. Shreenath, R. Trebino, J. M. Dudley, S. Coen, and R. S. Windeler, "Experimental studies of the coherence of microstructure-fiber supercontinuum," Opt. Express **11**(21), 2697–2703 (2003).

Optics EXPRESS

12. F. Lu and W. H. Knox, "Generation of a broadband continuum with high spectral coherence in tapered single-mode optical fibers," Opt. Express **12**(2), 347–353 (2004).
13. M. Bellini and T. W. Hänsch, "Phase-locked white-light continuum pulses: toward a universal optical frequency-comb synthesizer," Opt. Lett. **25**(14), 1049–1051 (2000).
14. A. Baltuska, M. Uiberacker, E. Goulielmakis, R. Kienberger, V. S. Yakovlev, T. Udem, T. W. Hansch, and F. Krausz, "Phase-controlled amplification of few-cycle laser pulses," IEEE J. Sel. Top. Quantum Electron. **9**(4), 972–989 (2003).
15. A.-L. Calendron, H. Çankaya, G. Cirmi, and F. X. Kärtner, "White-light generation with sub-ps pulses," Opt. Express **23**(11), 13866–13879 (2015).
16. L. Lepetit, G. Chériaux, and M. Joffre, "Linear techniques of phase measurement by femtosecond spectral interferometry for applications in spectroscopy," J. Opt. Soc. Am. B **12**(12), 2467–2474 (1995).
17. A. Borzsonyi, A. P. Kovacs, and K. Osvay, "What we can learn about ultrashort pulses by linear optical methods," Appl. Sci. **3**(2), 515–544 (2013).
18. N. Forget, L. Canova, X. Chen, A. Jullien, and R. Lopez-Martens, "Closed-loop carrier-envelope phase stabilization with an acousto-optic programmable dispersive filter," Opt. Lett. **34**(23), 3647–3649 (2009).
19. M. Natile, F. Guichard, Y. Zaouter, M. Hanna, and P. Georges, "Simple carrier-envelope phase control and stabilization scheme for difference frequency generation-based systems," Opt. Express **29**(11), 16261–16269 (2021).